

# High Temporal Resolution *XMM-Newton* Monitoring of PKS 2155–304

Rick Edelson<sup>1,2</sup>, Gareth Griffiths<sup>2</sup>, Alex Markowitz<sup>1</sup>, Steve Sembay<sup>2</sup>, Martin J. L. Turner<sup>2</sup>,  
Robert Warwick<sup>2</sup>

rae@astro.ucla.edu

## ABSTRACT

The bright, strongly variable BL Lac object PKS 2155–304 was observed by *XMM-Newton* for two essentially uninterrupted periods of  $\sim 11$  and 16 hr on 30–31 May 2000. The strongest variations occurred in the highest energy bands. After scaling for this effect, the three softest bands (0.1–1.7 keV) showed strong correlation with no measurable lag to reliable limits of  $|\tau| \lesssim 0.3$  hr. However, the hardest band ( $\sim 3$  keV) was less well-correlated with the other three, especially on short time scales, showing deviations of  $\sim 10$ – $20\%$  in  $\sim 1$  hr although, again, no significant interband lag was detected. This result and examination of previous *ASCA* and *BeppoSAX* cross-correlation functions suggest that previous claims of soft lags on time scales of 0.3–4 hr could well be an artifact of periodic interruptions due to Earth-occultation every 1.6 hr. Previous determinations of the magnetic field/bulk Lorentz factor were therefore premature, as these data provide only a lower limit of  $B\gamma^{1/3} \gtrsim 2.5$  G. The hardest band encompasses the spectral region above the high-energy break; its enhanced variability could be indicating that the break energy of the synchrotron spectrum, and therefore of the underlying electron energy distribution, changes independently of the lower energies.

*Subject headings:* BL Lacertae Objects: General — BL Lacertae Objects: Individual (PKS 2155–304) — Galaxies: Active — Methods: Data Analysis — X-rays: Galaxies

## 1. Introduction

Blazars (BL Lacertae objects and optically violently variable quasars) show strong and rapid  $\gamma$ -/X-ray variability. When combined with their observed large apparent luminosities, this indicates that the emission we observe is beamed towards us, as isotropic emission would have to be highly super-Eddington (e.g., Bregman 1990). Likewise, determining the interrelations between variations in different energy bands can define geometrical and causal relations between emission regions and processes. For instance, X-ray variations in the blazar PKS 2155–304 have been seen to lead those

---

<sup>1</sup>Astronomy Department; University of California; Los Angeles, CA 90095-1562; USA

<sup>2</sup>X-ray Astronomy Group; Leicester University; Leicester LE1 7RH; United Kingdom

in the optical/ultraviolet (e.g., Edelson et al. 1995, Urry et al. 1997), indicating that the X-rays are not produced by Compton scattering from these lower-energy bands.

In  $\sim 2$  day long *BeppoSAX* and *ASCA* monitoring of PKS 2155–304, Chiappetti et al. (1999), Zheng et al. (2000) and Kataoka et al. (2000) reported that variations in the soft X-ray band (0.1–1.5 keV) lagged behind those in the hard X-ray band (3.5–12 keV) by  $\sim 0.3$ –4 hr. These “soft lags” were explained as due to energy-dependent radiative cooling losses. Such small interband lags have been claimed in monitoring of Mkn 421, a similar type of blazar: Takahashi et al. (1996) found soft lags, Fossati et al. (2000) found hard lags, and Takahashi et al. (2000) found both hard and soft lags in a single very long observation. However, all of those observations were made with low-Earth orbit satellites, for which the input light curves were corrupted by Earth-occultation interruptions every  $\sim 1.6$  hr orbit, making highly problematic the unambiguous detection of short lags as discussed in § 4.1.

This paper reports the results of essentially continuous  $\sim 11$  and 16 hr *XMM-Newton* observations of PKS 2155–304. With its highly eccentric  $\sim 48$  hr orbit (permitting long uninterrupted viewing), high throughput and wide bandpass, *XMM-Newton* is ideally suited for reliably measuring small interband lags. The observations and data reduction are discussed in the next section, the temporal analysis is reported in § 3 and the results are discussed in § 4.

## 2. Observations and Data Reduction

### 2.1. Observations

PKS 2155–304 was observed during *XMM-Newton* orbit # 87, from 2000 May 30 05:28:29 UT to 2000 May 31 20:40:34 UT. Because this performance verification/guaranteed time observation occurred early in the mission, only a fraction of the currently available orbit was spent gathering data, and some of the instruments were in non-standard configurations that precluded time-series analysis. *XMM-Newton* (Jansen et al. 2001) made useful observations of PKS 2155–304 during two uninterrupted intervals, “Interval A,” which occurred before the  $\sim 4$  hr mid-orbit interruption, and “Interval B,” which occurred afterwards. Observation logs are given in Table 1.

Because this experiment required very high sensitivity in order to reach acceptable signal-to-noise ratio in the broadband flux in the shortest time and thus be sensitive to the smallest possible interband lags, only data from the high-throughput European Photon Imaging Camera (EPIC) instruments were considered. One of the EPIC instruments contains pn CCDs (Struder et al. 2001) while the other two comprise MOS CCDs (Turner et al. 2001). During Interval A, MOS1 was operated in partial window mode (PRI PART W4) and MOS2 in timing mode. During Interval B, MOS1 was operated in timing mode and MOS2 in PRI PART W4. In PRI PART W4 mode, only the central 100 x 100 pixels of the MOS central chip is read out, giving a frame integration time of  $\sim 0.15$  s and minimizing the effects of pileup. Also, the pn was in Small Window mode

for both intervals, yielding an integration time of  $\sim 5.7$  ms, again in order to prevent pileup. The medium filter was selected for all three instruments throughout. Due to current uncertainties in the calibration this paper does not consider timing mode data, so the Interval A MOS2 and Interval B MOS1 data were ignored.

## 2.2. Data Reduction

A standard reduction of raw pn and MOS event lists was performed using the Science Analysis System (SAS). This involved the subtraction of hot, dead or flickering pixels, removal of events due to electronic noise and correction of event energies for charge transfer losses. For the pn, only pattern 0 events were used while events with patterns 0-12 were selected for the MOS cameras. The pattern of an event defines the shape of the charge cloud created by that event, similar to *ASCA* “grades,” so the smaller pattern number means a more concentrated and therefore more reliable event (e.g., pattern 0 corresponds to a single pixel event).

X-ray light curves were accumulated for all three cameras from events extracted within a circle of radius  $45''$  around the source centroid. No background light curve was measured since the broadband source count rates are of order  $\sim 1000$  times the background. Exposure times of approximately 11 hr were obtained during Interval A and 16 hr during Interval B. The data were initially extracted in 3 s intervals, then rebinned to 0.167 hr (600 s) bins. At about May 30 19:15 and again at May 31 10:00, the pn shut down for  $\sim 0.1$  hr; values for these two points were derived by linear interpolation from the adjacent points. Light curves were extracted for the entire usable band (0.1-12 keV). The data were also broken up into four bands of 0.1-0.35 keV, 0.4-0.75 keV, 0.9-1.7 keV and 2.0-12.0 keV. These light curves, called VS (e.g., Very Soft), S, H and VH, respectively, form the basis of the analysis below.

## 3. Comparison of Hard and Soft Band Light Curves

The light curves are shown in Figure 1. The variability is lower than seen in some historical campaigns, but some of these were triggered e.g., by  $\gamma$ -ray flares, so they might be expected to show enhanced variability. Because PKS 2155–304 is so bright in the EPIC-pn ( $\sim 60$  ct/s), significant variations are seen above the  $\sim 1\%$  errors down to very short time scales ( $\sim 0.3$  hr).

### 3.1. Variability Amplitudes

An obvious feature of Figure 1 is that the strongest variability is seen in the hardest bands. The strong relation between energy band and variability level is confirmed in Table 2. The excess variance is defined as  $\sigma_{xs}^2 = (S^2 - \langle \sigma_{err}^2 \rangle) / \langle X \rangle^2$ , where  $S^2$  is the measured variance of the light

curve and  $\langle X \rangle$  and  $\langle \sigma_{err}^2 \rangle$  are the mean and mean square errors, respectively). The more intuitive fractional variability parameter is simply the square root of the excess variance:  $F_{var} = \sqrt{\sigma_{xs}^2}$ . Note that  $F_{var}$  increases monotonically and strongly with energy band, e.g., from 1.5% at  $\sim 0.2$  keV to 5.4% at  $\sim 3$  keV in Interval B.

The Interval B data are more useful because they cover a  $\sim 50\%$  longer time span and show stronger and sharper variations than Interval A. Also, the pn count rate is  $\sim 2.6$  times the MOS count rate and direct comparison of scaled pn and MOS data from the same energy bands and intervals showed excellent agreement within the errors. Thus, only the pn data are used in the following analysis, and the MOS are not used.

### 3.2. Cross-Correlation Analysis

The first step in the construction of a cross-correlation function (CCF) is to normalize the two light curves to zero mean and unit variance by subtracting the mean and dividing by the rms of the light curve. Plots scaled in this fashion provide an intuitive way to visualize the agreement between two light curves, as shown for two pairs of light curves in Figure 2.

#### 3.2.1. Correlations and Divergences Between the Light Curves

Figure 2 presents the most and least well-correlated pairs of light curves in this study. The H and S band light curves are essentially identical within the errors (Figure 2, top), and in fact all of the softest bands (0.1–1.7 keV) track well. However, the  $\sim 3$  keV VH band shows significant divergences, as is most clearly seen in the plot with the VS band (Figure 2, bottom). The VH band shows flare-like features that are not seen in other bands, with durations of  $\sim 1$  hr, at  $\sim 10:00$ – $12:00$  of Interval A and  $\sim 08:30$ – $10:30$  in Interval B. However, on longer time scales, the VH band does appear to track the three softer bands. Throughout all the light curves, there is no obvious tendency for variations in one band to lead those in another.

#### 3.2.2. Interband Lags

CCFs were measured using both the interpolated (ICF; White & Peterson 1994) and the discrete correlation functions (DCF; Edelson & Krolik 1989). Uncertainties in the ICF lags were estimated using the bootstrap method of Peterson et al. (1998). The CCF results are tabulated for all pairs of bands in Table 3, with the data ordered by descending  $r_{max}$  in the (better-defined) Interval B CCFs.

The CCFs shown in Figure 3, derived from the data in Figure 2, were chosen to cover the full range of data quality in this experiment. In the most useful interval (Interval B), the best-

correlated pair (H vs. S) show a classic sharp, single-peaked CCF, with a large correlation coefficient ( $r_{max} \approx 0.9$ ). These data are ideal for measuring lags, and in fact the measured lag is zero to within the errors. The formal 90% confidence limit is  $|\tau| \lesssim 0.12$  hr, but we assign a more conservative minimum  $2\sigma$  limit of twice the mean sampling bin, or in this case, 0.3 hr. We note that the other two soft CCFs (VS vs. S and VS vs. H) are also consistent with  $|\tau| \lesssim 0.3$  hr, so we assign this limit to Interval B lags throughout the soft bands. In Interval A, the light curve is shorter and the variations are not as sharp, and the peak is correspondingly less well-defined, with limits of only  $|\tau| \lesssim 0.6$  hr throughout the soft bands. In all but one of these cases, the mean lags are within the 90% confidence limits and of the 12 runs (six with the DCF and six with the ICF), five were positive, five were negative, and two were identically zero. Thus, we conclude that there is no evidence for soft or hard lags within the 0.1–1.7 keV band, to conservative limits of  $|\tau| \lesssim 0.3$  hr in Interval A and  $|\tau| \lesssim 0.6$  hr in Interval A.

Somewhat different behavior may be indicated by the VH vs. VS CCF. The Interval B data are not very strongly correlated ( $r_{max} \approx 0.64$ ), but they do show a well-defined albeit broad CCF peak. The limit on the interband lag is correspondingly worse,  $|\tau| \lesssim 1$  hr, and similarly weak limits are derived for the VH/S and VH/H CCFs. The Interval A CCF is even worse, showing two essentially equal broad peaks at about  $\pm 1$  hr, with a correlation coefficient of  $r_{max} \approx 0.57$ ). The formal limit on this CCF is also  $|\tau| \lesssim 1$  hr. Again, the ICF lags are within than the 90% confidence limits and of the 12 ICF and DCF runs, four were positive, seven were negative, and one identically zero. More importantly, the Interval A VH/VS CCF clearly fails a common-sense visual inspection of the CCF as neither peak is statistically more significant than the other. It is essentially unusable for time series analysis. That is, in the absence of the Interval B data, no conclusions whatsoever could be reached with the Interval A data alone.

## 4. Discussion

In this set of two uninterrupted *XMM-Newton* long-looks at PKS 2155–304, no evidence was found for soft interband lags (or for hard lags). The variability amplitude increases dramatically from soft to hard energies. After scaling for these differences, the soft band (0.1–1.7 keV) light curves track well, but the very hard band ( $\sim 3$  keV) light curve shows small but significant divergences with the soft bands on shorter time scales.

### 4.1. Comparison with Previous Observations

The lack of an interband lag appears to contradict previous claims of  $\sim 0.3$ –4 hr lags, based on monitoring by the low-Earth orbit telescopes *ASCA* in 1994 and *BeppoSAX* in 1996 and 1997. However, those  $\sim 2$  day observations had only  $\sim 50\%$  (or worse) duty cycles, suffering from Earth-occultation interruptions at the 1.6 hr orbital period that tremendously complicate the measure-

ment of short lags. The uninterrupted, high signal-to-noise *XMM-Newton* data do not have these problems.

These problems are clearly seen in the 1997 November *BeppoSAX* observation. Chiappetti et al. (1999) found that variations in the hard band (3.5–10 keV) led those in the soft band (0.1–1.5 keV) by  $0.5 \pm 0.08$  hr. However, the CCF (see Figure 3 of Chiappetti et al. 1999) shows a strong, periodic feature, with very large errors, large negative deviations, and/or missing data at, e.g.,  $-5.2$ ,  $-3.6$ ,  $-2.1$ ,  $-0.5$ ,  $+1.1$ ,  $+2.7$ ,  $+4.3$  hr. These occur at the satellite orbital period ( $\sim 1.6$  hr), as would be expected because both light curves suffer interruptions at this period due to Earth occultation. (The excursions/interruptions are asymmetric with respect to zero lag, possibly due to different acceptance criteria for the low and medium energy light curves that covered slightly different periods.) This systematic corruption of the CCF on short time scales makes it highly problematic to reliably measure lags  $\lesssim 1$  orbit. In this particular case, the asymmetry of the periodic artifact means that near zero lag, negative lags are more strongly biased down, shifting the center of weight of the CCF higher and producing the impression of a positive lag. Note also that the three highest points in this CCF (excluding the one very noisy point) are also the three closest to zero (with  $|\tau| \leq 0.2$  hr), and that the claimed lag actually lies near a local minimum in the CCF. The same effect is seen the Zheng et al. (2000) CCF derived from the same data (Figure 5a of that paper): a strong, asymmetric artifact with a 1.6 hr period. Again, although that paper claimed a soft lag of  $\sim 0.3$  hr, the three highest points indicate no measurable lag.

Likewise, both Zheng et al. (2000) and Kataoka et al. (2000) claimed soft lags of  $\sim 0.3$ – $1.1$  hr, increasing as the gap between the hard and soft bands was increased, in the 1994 *ASCA* data. Kataoka et al. (2000) did not show a CCF but that in Zheng et al. (2000; Figure 5e) is weak ( $r_{max} \approx 0.6$ ) and broad and consistent with any lag between  $-2$  and  $+4$  hr. Finally, a  $\sim 4$  hr soft lag was claimed in the 1996 *BeppoSAX* CCF (Zheng et al. 2000; Figure 5c), but that correlation is also weak ( $r_{max} \approx 0.7$ ) and broad, approximately constant for all lags between 0 and  $+4$  hr. That light curve was also corrupted by interruptions on longer ( $\sim 4$ – $6$  hr) time scales, possibly introducing artifacts on these time scales as well.

Interband lags have also been claimed in a similar HBL (see below), Mkn 421. Takahashi et al. (1996) found soft lags smaller than 1 orbit in an *ASCA* campaign, with the same sort of band-gap dependence claimed in the 1994 *ASCA* observations of PKS 2155–304. Fossati et al. (2000) found the opposite: that the hard band lagged behind the soft in a series of *BeppoSAX* observations. Finally, in a very long (11-d) *ASCA* observation, Takahashi et al. (2000) tentatively claimed that Mkn 421 exhibited both hard and soft X-ray lags, again on time scales of  $\lesssim 1$  orbit, but noted the possibility that the result could be spurious, caused by periodic Earth-occultation. CCFs were not shown in Takahashi et al. (1996, 2000), but they were in Fossati et al. (2000), and showed the same kind of periodic corruption as the 1997 PKS 2155–304 CCFs. Takahashi et al. (2000) found the detection of both hard and soft lags challenging to explain theoretically, but there is a simple observational explanation: that none of the lags, hard and soft, shorter than or of order the orbital interruption time scale, are real.

In summary, the limits on the interband lag in this campaign appear inconsistent or only marginally consistent with previous claims of soft (and hard) lags in this source and Mkn 421. However, direct examination of those CCFs indicate that they are in fact fully consistent with zero lag, and that claims of measurable lags could easily have resulted from periodic artifacts caused by Earth-occultation.

## 4.2. Theoretical Implications

Blazar SEDs have two distinct components, with one dominating at lower energies and peaking in the X-ray regime, and the other peaking in  $\gamma$ -rays. This suggests that there are two emission processes operating: incoherent synchrotron emission at lower energies and Compton scattering at higher energies. The possibility that the synchrotron photons could be the seeds for the Compton emission (the synchrotron self-Compton, or SSC process) is consistent with the data, but an unambiguous link has not been established. SED snapshots have been obtained for many blazars, which appear to segregate into two classes that may or may not be extrema of a single population: HBLs, for which the low-energy component peaks in the X-rays and dominates emission in that band, and LBLs, which peak at lower (ultraviolet/optical) energies and for which either the synchrotron or Compton component can dominate in the X-rays. HBLs tend to show no emission lines (while LBLs do) and to have lower luminosities than LBLs (e.g., Sikora et al. 1997). Both PKS 2155–304 and Mkn 421 (the other blazar for which soft lags are claimed) are HBLs, and are two of only five AGN (all HBLs) that have been detected at TeV energies.

A variety of models can fit these single-epoch SEDs (e.g., Ghisellini et al. 1998). These provide a framework for understanding blazar physics, but cannot fully exploit the potential constraints offered by the strong *variability* seen in blazars. Time-dependent models are being developed (e.g., Mastichiadas & Kirk 1998), but as of this writing they have focused on a few special cases and are not directly applicable to these data.

In the absence of such detailed models, these results still allow determination of some general constraints on the physical conditions in PKS 2155–304. Measurement of a soft lag could have given the cooling time scale and therefore an estimate of the magnetic field (assuming a value for the Lorentz factor  $\delta$ ), assuming that the lag is due to the electron population softening as the hard electrons preferentially lose energy due to radiative losses by the following formula (from Chiappetti et al. (1999)):

$$B\delta^{1/3} = 300 \left( \frac{1+z}{\nu_1} \right)^{1/3} \left( \frac{1 - (\nu_1/\nu_0)^{1/2}}{\tau} \right)^{2/3} \text{ G}, \quad (1)$$

where  $B$  is the magnetic field strength,  $z$  is the redshift, and  $\nu_1$  and  $\nu_0$  are the frequencies (in units of  $10^{17}$  Hz) at which the lag,  $\tau$ , is measured. Because this experiment only yielded an upper limit on  $\tau$ , only a lower limit can be obtained for  $B\delta^{1/3}$ . For the parameters measured in the H/S CCF,  $z = 0.12$ ,  $\nu_0 = 3$ ,  $\nu_1 = 0.5$  (1.2 and 0.2 keV, respectively), and  $\tau \lesssim 1000$  s, we derive a lower limit of  $B\delta^{1/3} \gtrsim 2.5$  G. A similar constraint is obtained with the 1/4 CCF data: the band gap is

larger, with  $\nu_0 = 7$  and  $\nu_1 = 0.5$  (3 and 0.2 keV, respectively), but the limit on the lag is much worse,  $\tau \lesssim 4000$  s, so a less stringent limit of  $B\delta^{1/3} \gtrsim 1.3$  G is derived. These limits are marginally inconsistent with those based on the claimed detection of an interband lag, e.g.,  $B\delta^{1/3} = 2.5$  G (Kataoka et al. 2000).

Perhaps the most interesting result of this experiment is that the VH ( $\sim 3$  keV) band shows significant differences with the three softer bands (0.1–1.7 keV) on time scales of  $\lesssim 1$  hr. The time-averaged spectrum of PKS 2155–304 shows a break between these bands, steepening from  $\Gamma \approx 2.45$  to  $\Gamma \approx 2.7$  at about  $\sim 2$  keV. This means that the VH band would be sensitive to changes in the break energy. The fact that the variations in this band are much more pronounced than, and relatively less correlated with those in the softer (power-law) part of the spectrum could indicate that the peak of the synchrotron spectrum is changing in a manner unrelated to the changes in the normalization. As the peak of the spectrum corresponds to the maximum energy in the power-law distribution of electrons, this could be indicating that the heating time scale is becoming comparable to the light-crossing time scale at these energies. However, this effect needs to be firmly established and explored in greater detail, e.g., by extended *XMM-Newton* monitoring of this source and Mkn 421, the other blazar for which short lags have been claimed, and the brightest in the sky.

The authors thank the *XMM-Newton* team, especially at Leicester and Vilspa, for the smooth operation of this new, complex and very powerful instrument. They also appreciate Greg Madejski and Laura Maraschi for discussions that aided greatly their understanding of blazar physics and preparing of the observing proposal. Edelson thanks the people of Vietnam for their hospitality while this paper was being written. Edelson and Markowitz were supported by NASA grants NAG 5-7317 and NAG 5-9023.

## REFERENCES

- Bregman, J. 1990, *Astronomy and Astrophysics Review* (ISSN 0935-4956), v. 2, no. 2, p. 125-166  
 Chiappetti, L. et al. 1999, *ApJ*, 521, 552  
 Edelson, R., Krolik, J. 1989, *ApJ*, 333, 646  
 Edelson, R. et al. 1995, *ApJ*, 438, 120  
 Fossati, G. et al. 2000, *ApJ*, in press (astro-ph/0005066)  
 Ghisellini, G. et al. 1998, *MNRAS*, 301, 451  
 Jansen, F., Lumb, D., Altieri, B., et al. 2001, *A&A*, 365, in press  
 Kataoka, J. et al. 2000, *ApJ*, 528, 243  
 Mastichiadis, A., Kirk, J. 1997, *A&A* 320, 19  
 Peterson, B. M. et al. 1998, *PASP*, 110, 660

- Sikora, M. et al. 1997, ApJ, 484, 108  
Strüder, L., Briel, U. G., Dennerl, K., et al. 2001, A&A, 365, in press  
Takahashi, T. et 1996, ApJL, 470, L79  
Takahashi, T. et 2000, ApJ, in press (astro-ph/0008505)  
Turner, M. J. L., Abbey, A., Arnaud, M., et al. 2001, A&A, 365, in press (astro-ph/0011498)  
Urry, C. M. et al. 1997, ApJ, 486, 799  
White, R., Peterson, B. M. 1994, PASP, 106, 879  
Zheng, Y. et al. 1999 ApJ, 527, 719

---

This preprint was prepared with the AAS L<sup>A</sup>T<sub>E</sub>X macros v5.0.

Table 1. Observing Log

Interval	Instrument	Obs. Period (2000 May UT)
A	pn	30 10:20:09 – 30 20:53:29
A	MOS1	30 10:58:41 – 30 21:53:42
B	pn	31 00:52:59 – 31 17:21:38
B	MOS2	31 01:32:15 – 31 17:20:29

Table 2. Variability Parameters

Camera	Band (keV)	Band Ctr. (keV)	Int. A ct/s	Int. A $F_{var}$ (%)	Int. A $\sigma_{xs}^2$ ( $\times 10^{-4}$ )	Int. B ct/s	Int. B $F_{var}$ (%)	Int. B $\sigma_{xs}^2$ ( $\times 10^{-4}$ )
pn	0.1–12	0.7	61.4	1.9	3.7	60.6	2.4	5.7
pn	0.1–0.35	0.2	20.5	1.1	1.2	19.8	1.5	2.4
pn	0.4–0.75	0.6	18.7	1.9	3.8	18.4	2.3	5.1
pn	0.9–1.7	1.2	10.4	2.8	8.1	10.5	3.4	11.8
pn	2.0–12	3	2.7	4.2	17.9	2.9	5.4	28.7
MOS	0.1–12	0.7	23.2	2.6	6.7	23.8	2.8	7.6
MOS	0.1–0.35	0.2	4.6	1.4	1.9	4.7	1.5	2.2
MOS	0.4–0.75	0.6	6.1	2.5	6.1	6.2	2.1	4.5
MOS	0.9–1.7	1.2	6.4	3.2	10.3	6.6	3.5	12.0
MOS	2.0–12	3	2.1	4.4	19.3	2.3	5.1	25.5

Table 3. Cross-Correlation Results

Band 1 (keV)	Band 2 (keV)	Interval	DCF $r_{max}$	DCF $\tau$ (hr)	ICF $r_{max}$	ICF $\tau$ (hr)
0.4–0.75	0.9–1.7	A	0.85	0.00	0.88	+0.08 $\pm$ 0.50
0.1–0.35	0.4–0.75	A	0.74	–0.83	0.77	–0.75 $\pm$ 0.46
0.1–0.35	0.9–1.7	A	0.71	–0.50	0.75	–0.42 $\pm$ 0.69
0.9–1.7	2.0–12	A	0.78	+0.17	0.82	+0.08 $\pm$ 0.69
0.4–0.75	2.0–12	A	0.70	0.00	0.75	+0.08 $\pm$ 1.08
0.1–0.35	2.0–12	A	0.56	+0.50	0.59	–0.92 $\pm$ 1.00
0.4–0.75	0.9–1.7	B	0.89	–0.17	0.91	–0.08 $\pm$ 0.12
0.1–0.35	0.4–0.75	B	0.80	+0.33	0.84	+0.25 $\pm$ 0.29
0.1–0.35	0.9–1.7	B	0.78	+0.17	0.82	+0.25 $\pm$ 0.31
0.9–1.7	2.0–12	B	0.76	0.00	0.79	–0.08 $\pm$ 0.17
0.4–0.75	2.0–12	B	0.74	–0.33	0.77	–0.25 $\pm$ 0.64
0.1–0.35	2.0–12	B	0.62	–0.50	0.65	–0.25 $\pm$ 1.08

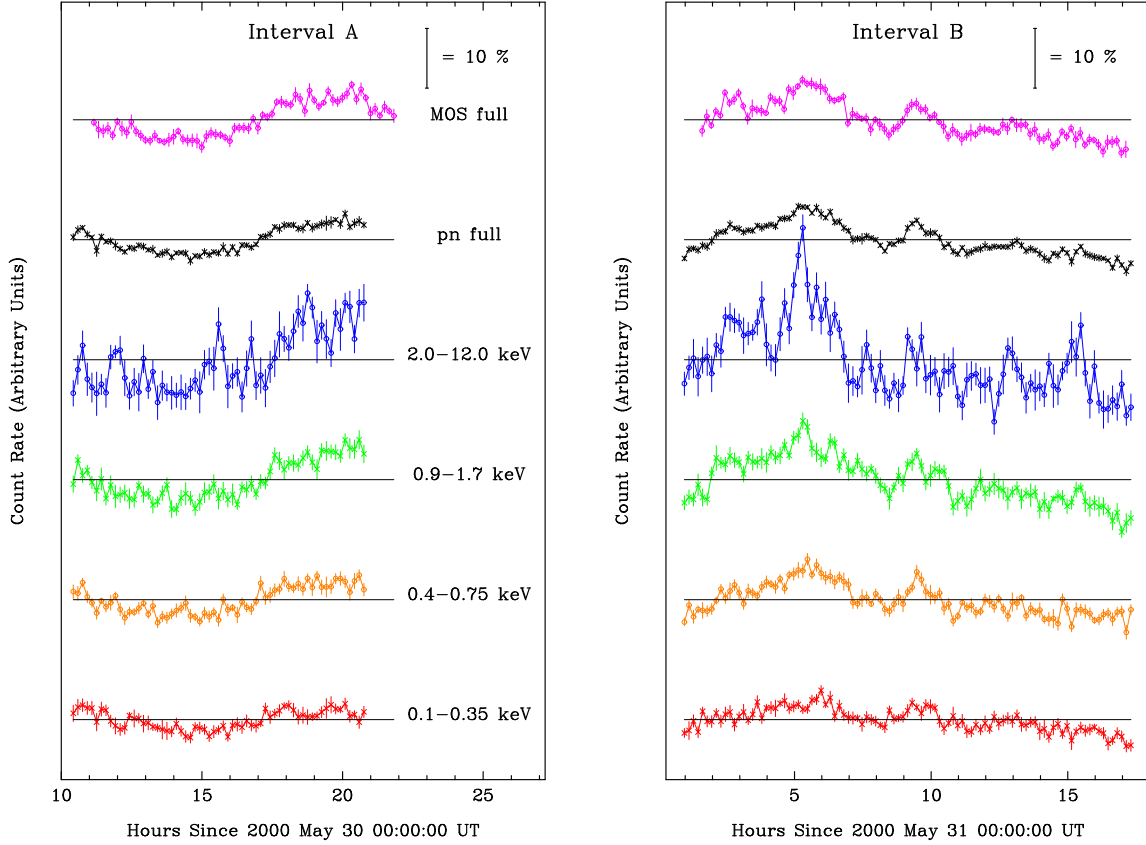


Fig. 1.— *XMM-Newton* light curves for PKS 2155–304, for Interval A (left) and Interval B (right). The data are binned in 0.167 hr intervals, and a logarithmic y-axis is used. From top to bottom, count rates are given for the MOS total (0.1–12 keV), pn total (0.1–12 keV), and four pn subbands (2.0–12, 0.9–1.7, 0.4–0.75 and 0.1–0.35 keV, or VH, H, S and VS, respectively).

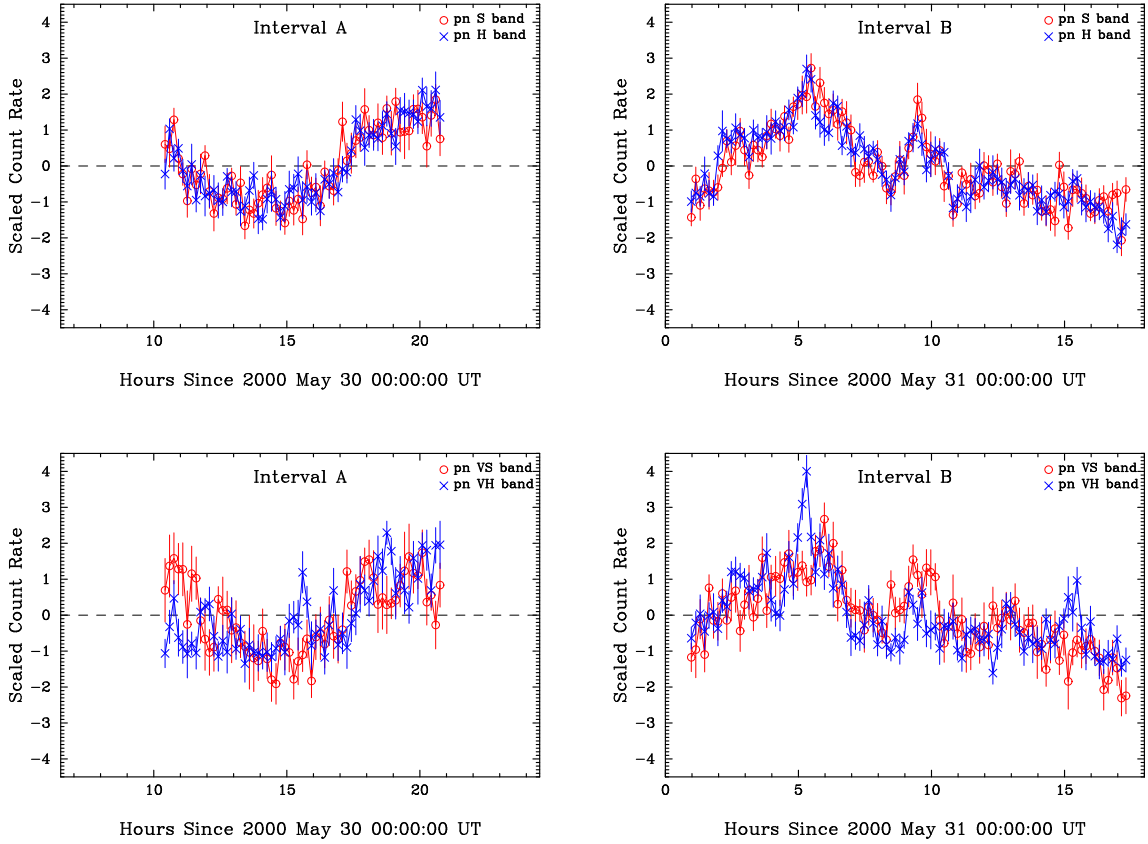


Fig. 2.— Scaled PKS 2155–304 pn soft (circles) and hard band ( $\times$ s) light curves. Data are shown for bands H/S (top) and VH/VS (bottom), over Interval A (left) and Interval B (right). The data in each band first had the mean count rate subtracted, and then were divided by the rms (that is, the standard initial scaling before performing the CCF), so that they have the same apparent means and variances. Note how well the H and S light curves track each other, and that the VH and VS light curves track well on long time scales, although significant detailed differences can be seen between the VH and VS bands on short time scales.

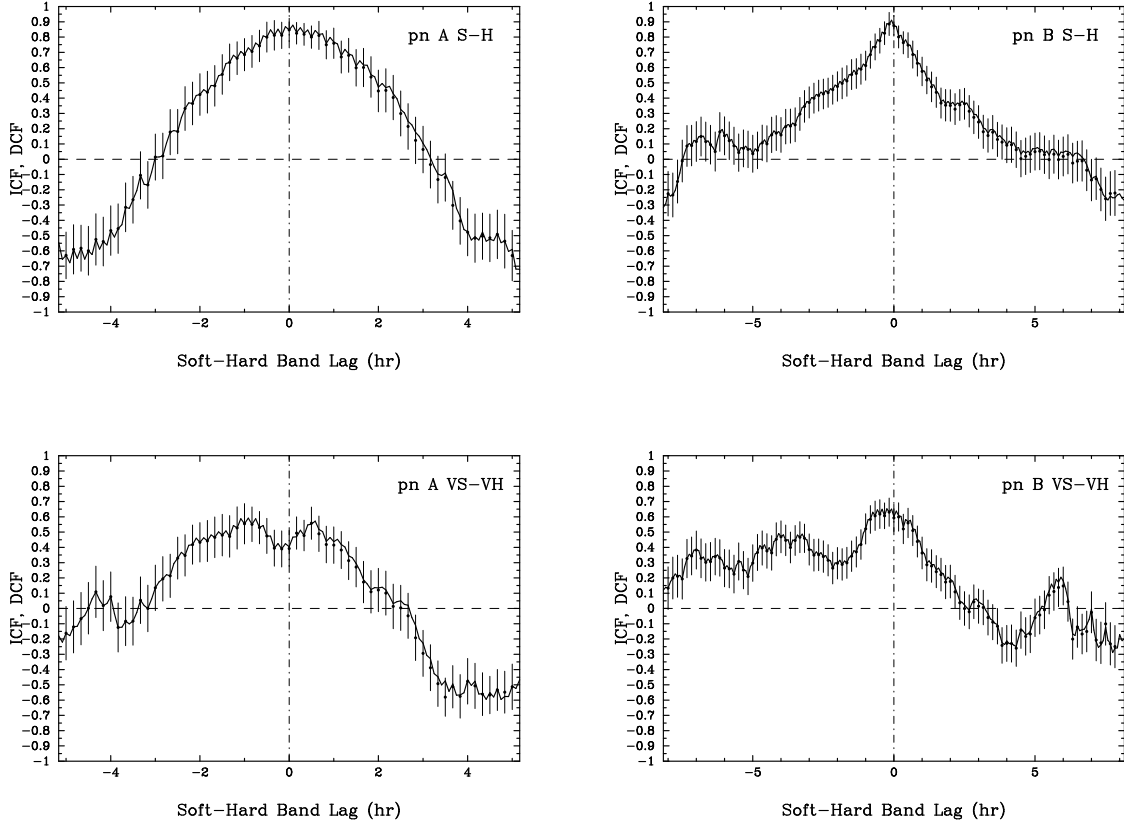


Fig. 3.— CCFs for bands H/S (top) and VH/VS (bottom), over Interval A (left) and Interval B (right). The DCF, shown as circles with error bars, was binned at the natural time scale of the input light curve, 0.167 hr. The ICF, shown as a solid line, is binned on a time scale of 0.067 hr. All of the measured CCFs are consistent with zero lag, with no tendency for one band to lead the other. Note the range of quality in the CCFs, with the H/S Interval B data showing a strong sharp peak ( $r_{max} \approx 0.9$ ) yielding a formal limit of  $\tau \lesssim 0.12$  hr (although this paper adopts a more conservative limit of  $\tau \lesssim 0.3$  hr), while the Interval A VS/VH CCF is essentially unusable because it has two poorly defined, nearly equal peaks of  $r_{max} \approx 0.57$ .